

τ Boo b: Hunting for reflected starlight[★]

F. Rodler^{1,2,3}, M. Kürster⁴, and T. Henning⁴

¹ Instituto de Astrofísica de Canarias, C/Vía Láctea s/n, 38205 La Laguna, Spain

² formerly at the Max-Planck-Institut für Astronomie, Königstuhl 17, 69117 Heidelberg, Germany

³ formerly at the Institut für Astronomie, Universität Wien, Türkenschanzstrasse 17, A-1180 Vienna, Austria

⁴ Max-Planck-Institut für Astronomie, Königstuhl 17, 69117 Heidelberg, Germany

Received ?; accepted ?

ABSTRACT

Aims. We attempt to detect starlight reflected from the hot Jupiter orbiting the main-sequence star τ Boo, in order to determine the albedo of the planetary atmosphere, the orbital inclination of the planetary system and the exact mass of the planetary companion.

Methods. We analyze high-precision, high-resolution spectra, collected over two half nights using UVES at the VLT/UT2, by way of data synthesis. We interpret our data using two different atmospheric models for hot Jupiters.

Results. Although a weak candidate signal appears near the most probable radial velocity amplitude, its statistical significance is insufficient for us to claim a detection. However, this feature agrees very well with a completely independently obtained result by another research group, which searched for reflected light from τ Boo b. As a consequence of the non-detection of reflected light, we place upper limits to the planet-to-star flux ratio at the 99.9% significance level. For the most probable orbital inclination around $i = 46^\circ$, we can limit the relative reflected radiation to be less than $\epsilon = 5.7 \times 10^{-5}$ for grey albedo. This implies a geometric albedo smaller than 0.40, assuming a planetary radius of $1.2 R_{\text{Jup}}$.

Key words. Methods: data analysis – Techniques: radial velocities – Stars: individual: τ Boo – planetary systems

1. Introduction

Since the detection of the first exoplanet orbiting a solar-type star, more than 400 exoplanets have been detected. The existence of most of these planets was established by monitoring radial velocity (RV) variations of the host star, originating from the gravitational pull of the unseen planetary companion. So-called hot Jupiters are giant planets only a few solar radii away from their host stars that provide the opportunity to attempt the detection of starlight reflected from these planets. Five extended campaigns for the search for reflected light by using high-resolution spectroscopy were completed by different groups (Charbonneau et al. 1999, Collier Cameron et al. 1999, Collier Cameron et al. 2002, Leigh et al. 2003a., Leigh et al. 2003b, Rodler et al. 2008). Apart from Collier Cameron et al. (1999), who claimed a detection of reflected starlight, which was later withdrawn (Collier Cameron et al. 2000), all campaigns resulted in a non-detection of reflected starlight, and upper limits to the planet-to-star flux ratio and to the geometric albedo of these planets were established: to date, the tightest 99.9% confidence upper limits on the geometric albedos of the hot Jupiters τ Boo b, HD 75289b and ν And b are 0.39 (Leigh et al. 2003a), 0.46 (Rodler et al. 2008), and 0.42 (Collier Cameron et al. 2002), respectively. These results provided important constraints on models of the planetary atmospheres such as those by Sudarsky et al. (2000, 2003). As a result, models that predicted a high reflectivity for the planetary atmosphere could be ruled out for some of the studied planets.

More recently, the albedos of several transiting hot Jupiters at visual wavelengths could be further constrained from measurements of the secondary transit events. For the transiting hot

Jupiter HD 209458b, Rowe et al. (2008) placed a very stringent 3σ upper limit on the geometric albedo of 0.17 in the wavelength regime of 400-700 nm. Using data of the CoRot-satellite of the transiting hot Jupiter CoRot-1b, Snellen et al. (2009) measured a phase-dependency of the planetary flux and reported an upper limit on the geometric albedo of 0.2 in the wavelength range of 400-1000 nm. This upper limit of the geometric albedo of CoRot-1b was confirmed by an independent analysis by Alonso et al. (2009a). Using the same data set for the same target, Rogers et al. (2009) reports an estimate of the planetary geometric albedo to be 0.05. Alonso et al. (2009b) placed a very stringent upper limit on the geometric albedo of 0.06 of the hot Jupiter CoRot-2b in the wavelength range 400-1000 nm. The analysis of measurements of the secondary eclipse of the hot Jupiter HAT-P-7b with the EPOXI spacecraft and the Kepler-satellite led to an estimate of the geometric albedo of 0.13 at 650 nm (Christiansen et al. 2009). Measurements of the secondary transit of the planet Ogle-Tr-56 in the z' -band indicate a low geometric albedo less than 0.15 (Sing & Morales 2009). For a general summary of the secondary transit measurements we refer to Cowan & Agol (2010).

τ Boo^{tis} (HD 120136A) is a main-sequence star of spectral type F7, located at a distance of 15.6 pc from our Solar System. Butler et al. (1997) detected a massive hot Jupiter orbiting τ Boo via RV measurements; we note that this star is one of the brightest stars in the sky harboring a planet. Shortly after the discovery of the planetary companion, two research groups started campaigns for the search for reflected light by way of high-precision spectroscopy, which finally resulted in non-detections. The tightest published 99.9% confidence upper limit to the geometrical albedo is $p < 0.39$ under the assumption that the planetary radius $R_p = 1.2 R_{\text{Jup}}$, orbital inclination values $i \geq 36^\circ$ and grey albedo (Leigh et al. 2003a). These authors report the detection

Send offprint requests to: frodler@iac.es

[★] Based on observations made with ESO Telescopes at the Paranal Observatory under programme ID 079.C-0413(A).

of a candidate signal of marginal significance with a projected orbital RV semi-amplitude $K_p = 97 \text{ km s}^{-1}$, which corresponds to an orbital inclination $i \approx 40^\circ$.

Here, we present our analysis of new observations of the planetary system of τ Boo taken with the UV-Visual Echelle Spectrograph (UVES) mounted on the VLT/UT2 at Cerro Paranal in Chile. Section 2 describes the basic ideas of the search for reflected light. Section 3 provides an overview over the planetary system, while Section 4 outlines the acquisition and reduction of the high-resolution spectra. Section 5 provides a detailed description of the data analysis with a data modeling approach. Finally, in Section 6 we present the results, which are discussed in Section 7.

2. Starlight reflected from the planet

High resolution spectroscopic searches utilize the fact that the spectrum reflected from the planet is essentially a copy of the rich stellar absorption line spectrum except for the following differences:

- It is scaled down in intensity by more than five orders of magnitude in the visual for hot Jupiters (Section 2.1).
- It is shifted in wavelength according to the relative orbital radial velocity of the planet (Section 2.2).
- It displays a different degree of rotational broadening corresponding to the rotational velocity of the star as seen from the hot Jupiter whose own rotation typically contributes very little to the line broadening (Section 2.3)

2.1. Photometric Variations

For exoplanets, the enormous brightness contrast between the star and the planet constitutes a considerable challenge when attempting to observe some kind of direct signal from the planet. For close-in planets, such as hot Jupiters, the main contribution to the flux in the visual consists of the reflected starlight and not the intrinsic luminosity (Seager & Sasselov 1998).

According to Charbonneau et al. (1999), the amount of starlight reflected from a planet which is fully illuminated can be described by

$$\epsilon(\lambda) = p(\lambda) \left(\frac{R_p}{a} \right)^2, \quad (1)$$

where $p(\lambda)$ denotes the albedo of the planet as a function of the wavelength λ , R_p the planetary radius and a the star-planet separation. The planetary radius of τ Boo b is unknown; it can, however, be estimated from a comparison with the transiting planets, which provide an exact determination of their masses and radii (Bakos et al. 2007). The orbital radius is tightly constrained through Kepler's third law.

As the planet orbits its star, the fraction of the illuminated part of the planet changes relatively to the observer. Consequently, the observed reflected light is reduced, depending on the model describing the scattering behaviour of the atmosphere, its orbital inclination $i \in [0^\circ, 90^\circ]$ and the orbital phase $\phi \in [0, 1]$ of the planet. We note that we adopt the convention that $\phi = 0$ represents inferior conjunction of the planet (for $i = 90^\circ$, it would be the transit position). Lacking observational data for hot Jupiters we apply an empirical scattering model of the atmospheres of Jupiter and Venus (Hilton 1992), which can be approximated by

$$\mu(\phi, i) = 10^{-0.4\zeta(\alpha)}, \quad (2)$$

where

$$\zeta(\alpha) = 0.09 \left(\frac{1.8 \alpha}{\pi} \right) + 2.39 \left(\frac{1.8 \alpha}{\pi} \right)^2 - 0.65 \left(\frac{1.8 \alpha}{\pi} \right)^3 \quad (3)$$

and the phase angle α is given by

$$\cos \alpha = -\sin i \cos 2\pi\phi. \quad (4)$$

Finally, the flux of the reflected light from the planet at the orbital phase ϕ follows from Equations 1 and 2:

$$f(\phi, i, \lambda) = \epsilon(\lambda) \mu(\phi, i). \quad (5)$$

2.2. Doppler shifts

The planet orbiting its host star does not only produce a flux variation (Equation 5), but also a Doppler shift of the stellar spectrum reflected from the planet. The RV semi-amplitude K_p of that shift depends on the orbital inclination i , which is unknown for non-transiting planets. K_p can be expressed by

$$K_p = K_s \frac{M_s}{M_p \sin i} \sin i, \quad (6)$$

where K_s is the RV semi-amplitude of the star, and M_s and $M_p \sin i$ are the stellar mass and the minimum mass of the planet, respectively. The largest possible amplitude $K_{p,\max}$ occurs at orbital inclination $i = 90^\circ$ (Figure 1).

The instantaneous RV shift of the planetary signal with respect to the star depends on the orbital phase ϕ ,

$$V_p = K_p \sin 2\pi\phi. \quad (7)$$

2.3. Rotational broadening

As the star rotates, each absorption line is subjected to Doppler broadening since individual points on the visible disk of the star have different instantaneous radial velocity. Equation 8 describes the projected rotational velocity of the star:

$$v_{\text{proj},\star} = v_\star \sin i = 2\pi \sin i \frac{R_\star}{P_{\text{rot},\star}}, \quad (8)$$

where R_\star and $P_{\text{rot},\star}$ are the stellar radius and the rotation period of the star, respectively. If the inclination of the rotational axis is unknown, the true velocity v of the star remains unknown.

Mathematically, the rotational broadening constitutes a convolution of the intrinsic stellar line profile with a half ellipse whose width is equal to $\pm v \sin i$ (Gray 1992). The $v \sin i$ of the reflected stellar absorption lines, as they could be observed from the planet, can be calculated by way of Equation 9:

$$v_{\star,p} = 2\pi R_\star \left(\frac{1}{P_{\text{rot},\star}} - \frac{1}{P_{\text{orb}}} \right), \quad (9)$$

where P_{orb} is the orbital period of the planet. Equation 9 is based on the assumption that the orbital plane and the stellar equator are co-aligned. Analyses of Rossiter-McLaughlin effect RV-curves (Rossiter 1924; McLaughlin 1924) in transiting planets have shown that such a spin-orbit alignment is the case for the majority of the monitored systems (Fabricky & Winn 2009), although such systems have been recently discovered (e.g. Pont et al. 2009, Narita et al. 2009).

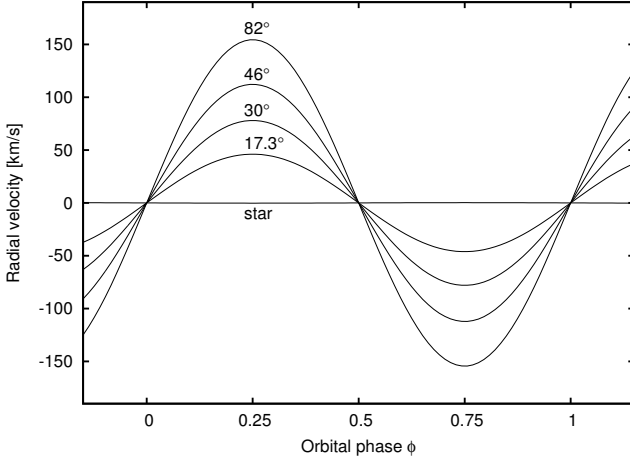


Fig. 1. RV curves of the planet orbiting τ Boo for selected orbital inclinations i . The maximum possible RV-shift of $K_p = 156 \text{ km s}^{-1}$ occurs at $i = 90^\circ$. For lower inclinations, the mass of the companion has to be larger to produce the stellar reflex motion with an RV semi-amplitude $K_s = 0.4611 \text{ km s}^{-1}$. The most probable orbital inclination is $i = 46^\circ$ under the assumption of a tidally locked system. The orbital inclination of $i = 82^\circ$ is the upper limit, coming from the non-transit detection, whereas $i = 30^\circ$ is the lower limit. For $i \leq 17.2^\circ$, the companion would exceed the mass of $13 M_{\text{Jup}}$ and therefore be a brown dwarf.

To calculate the broadening coming from the planetary rotation, we use Equation 10

$$v_{\text{proj,p}} = v_p \sin i = 2\pi \sin i \frac{R_p}{P_{\text{rot,p}}}, \quad (10)$$

where R_p is the planetary radius and $P_{\text{rot,p}}$ the planetary rotation period. We note that this equation is based on the assumptions that the planetary rotation axis is co-aligned with the orbital inclination axis, which is furthermore co-aligned with the stellar rotational axis. We justify these assumptions by the following argument: Close-in planets such as hot Jupiter seem to be tidally locked with their parent stars (c.f. Shkolnik et al. 2005; Knutson et al. 2007). A tidal lock hypothesis suggest that the orbital inclination is co-aligned with the planetary rotation axis and with the stellar rotation axis. The latter assumption was confirmed by the aforementioned spin-orbit measurements of transiting planets.

The two contributions $v_{\star,p}$ (Equ. 9) and $v_{\text{proj,p}}$ (Equ. 10) to the broadening are finally summed up to

$$v_{\text{refl}} = \sqrt{v_{\star,p}^2 + v_{\text{proj,p}}^2}. \quad (11)$$

3. τ Boo and its planet

Table 1 summarizes the parameters of the planet and its host star. We note in passing that the system also contains a faint M-dwarf component at a separation of $\approx 230 \text{ AU}$ from the primary (Patience et al. 2002; Eggenberger et al. 2003).

3.1. Radial velocity amplitude and orbital inclination

Knowing the stellar mass M_\star , the planetary minimum mass $M_p \sin i$, and the RV semi-amplitude of the reflex motion of the star K_\star , the RV semi-amplitudes of the planet can be constrained

Table 1. Parameters of the star τ Boo and its planetary companion. Abbreviations for the references are: B06 = Butler et al. (2006) and references therein, B97 = Baliunas et al. (1997), G98 = Gonzalez (1998), H00 = Henry et al. (2000), L89 = Latham et al (1989), L03 = Leigh et al. (2003a), VF05 = Valenty & Fischer (2005).

Parameter	Value	Error	Ref.
Star:			
Spectral type	F7 IV-V		B97
V (mag)	6.35		VF05
d (pc)	15.60	0.17	VF05
M_\star (M_\odot)	1.33	0.11	VF05
R_\star (R_\odot)	1.31	0.06	G98
P_{rot} (d)	3.31		B97
$v \sin i$ (km s^{-1})	14.9	0.5	H00
Age (Gyr)	1.3	0.4	VF05
Planet:			
$M_p \sin i$ (M_{Jup})	4.13	0.34	B06
a (AU)	0.0481	0.0028	B06
e	0.023	0.015	B06
K_\star (km s^{-1})	0.4611	0.0076	B06
Orbital period (d)	3.31245	0.00003	L03
$T_{\phi=0}$ (JD)	2 451 653.968	0.015	L03

to ranging from $K_p = 0$ to $155.6 \pm 18.3 \text{ km s}^{-1}$ (Equation 6; Figure 1).

Due to the absence of transits in high-precision photometry (Henry et al. 2000), we can constrain the range of possible orbital inclinations. The minimum orbital inclination i that a transit event occurs can be calculated by

$$\cos i = \frac{R_\star + R_p}{a}, \quad (12)$$

where R_\star and R_p is the stellar and the planetary radius, respectively, and a the semi-major axis. Using the parameters listed in Table 1, and the assumption that $R_p = 1.2 R_{\text{Jup}}$, we can exclude orbital inclinations of $i > 82^\circ$ for τ Boo b.

Baliunas et al. (1997) found that the star τ Boo rotates rapidly with a period commensurate with the orbital period of the planet, suggesting tidal locking. This hypothesis seems to be very likely for close-in planets (e.g. Shkolnik et al. 2005; Knutson et al. 2007), but has not been observationally confirmed so far. A tidal lock enables us to place an estimate on the orbital inclination (Equation 13) under the assumption that the stellar equator and the orbital plane are co-aligned.

In order to calculate the orbital inclination, we need to solve

$$\sin i = \frac{v_{\text{proj},\star}}{v_\star} = \frac{v_{\text{proj},\star} P_{\text{rot},\star}}{2\pi R_\star}, \quad (13)$$

where v_\star is the measured rotational velocity of τ Boo ($v_{\text{proj},\star} = v_\star \sin i = 14.9 \text{ km s}^{-1}$) for the unknown orbital inclination i , and v the true, but unknown rotational velocity. This rotational velocity v_\star can be estimated by way of Equation 8, which requires the knowledge of the stellar radius and stellar rotation period. Adopting the parameters listed in Table 1, we determine the maximum rotational velocity of the star to be $v_\star = 20.0 \pm 10 \text{ km s}^{-1}$. This gives an orbital inclination of $i = 46_{-16}^{+36}^\circ$. The resulting mass of the companion to τ Boo of $M_p = 5.7_{-1.5}^{+2.6} M_{\text{Jup}}$ would clearly confirm the planet hypothesis. We note that the error values of i and M_p correspond to the maximum error range.

3.2. Rotational broadening

We investigated how the reflected spectrum from the planet would be affected by a tidal lock and planetary rotation, using the following assumptions: The hot Jupiter orbiting τ Boo rotates in ≈ 3.1 days (1:1 resonance with the orbital motion), and the rotation axis is co-aligned with that of the star. In addition, the rotation of the planet is assumed to be prograde, and the planetary radius is $R_p = 1.2 R_{\text{Jup}}$.

A tidal lock causes that an imaginary observer sitting on the planets always sees the same side of the star; the star appears to be non-rotating. For this reason, $v_{\star,p} = 0 \text{ km s}^{-1}$. According to Equation 10, we find that the reflected absorption lines from the planet are broadened by approximately $v_p \sin i = 2 \text{ km s}^{-1}$. In order to estimate the resulting full width at half maximum (FWHM) of the reflected stellar absorption lines, we investigate slowly rotating stars of similar spectral type.

A very good candidate is the star HD 136351 (spectral type: F6 IV), which shows a rotational broadening of $v_{\star} \sin i = 2.8 \text{ km s}^{-1}$ (Reiners & Schmidt 2003). The average FWHM of the absorption lines is 12 km s^{-1} . Since the rotational velocity of the planet is estimated to be smaller (see above), we estimate the resulting FWHM of the reflected stellar absorption lines to be about 11.8 km s^{-1} .

4. Data acquisition and data reduction

We observed τ Boo during two consecutive nights in June 2007 using UVES (Dekker et al. 2000) mounted on the VLT/UT2 and collected a total of 406 high-resolution spectra (Table 2). In addition to that, we took spectra of the slowly rotating star HD 136351 and the rapidly rotating B-star HD 116087 ($v_{\star} \sin i = 241 \text{ km s}^{-1}$; Hoffleit & Jaschek 1991). The latter star was observed for the identification of telluric features in the red part of the visual. The dates of the observations were selected in such a way that the observations were carried out at orbital phases at which the planetary signal was strongest, i.e. close to the position of superior conjunction, which would be the secondary transit in case of $i = 90^\circ$. We aimed at taking observations in the phase ranges $\phi = 0.30$ to 0.45 and 0.55 to 0.70 , but avoiding $\phi = 0.50$ because of intense blending of the planetary and stellar absorption lines.

The observations were conducted using the red arm of UVES with a non-standard setting centered at wavelength $\lambda = 430 \text{ nm}$ providing 47 full orders and covering the wavelength range $\lambda = 425$ to 632 nm . We observed through a $0.3''$ slit and the image slicer IS#3, providing us a spectral resolution of $R = \lambda/\Delta\lambda = 110\,000$. The integration time for our target was selected to provide the maximum count rate but at the same time avoiding to reach the non-linear regime of neither one of the two CCDs. The exposure times for our bright target ranged between 60 and 400 s (120 s on average) and 30 and 60 s (40 s on average), respectively for the first and the second night. We carried out our observations in the fast-R/O mode; the total dead-time between two exposures was 16 s. Due to clouds and thick cirrus, we only collected half of the expected spectra.

In addition to the science frames, we obtained a large number of calibration exposures. Before the start of the first night, we took 163 flat-field and 104 bias exposures. In the afternoon before the second night, we collected 245 flat-field and 65 bias exposures. The large number of calibration frames was important to achieve a low photon noise in the finally combined flat-field frame (masterflat).

4.1. Data reduction

In order to prevent introducing data reduction artefacts to the data, we aimed at keeping the spectra as raw as possible. Consequently, we only adopted the absolutely necessary data reduction steps, as pointed out in the following. Effects like errors in the wavelength calibration, trends in the continuum, instrumental profile changes were considered in the model for the star/planet (see Section 5).

In the first step, we created masterbias frames for each night, being the median of all bias exposures per night. These masterbias frames were then subtracted from the science frames as well as from the flat-field frames. The error of the flux in the science frames was determined on the basis of Poisson statistics and propagated in the further data analysis steps. In the following step, for each night the flat-field exposures were scaled with their inverse exposure times and then combined into their median (masterflat) to permit high-quality flat-field correction in order to compensate for sensitivity variations of the pixels. The science frames were divided by the appropriate masterflat. Since both the flat-field frames as well as the object frames show a similar Blaze function, this function was then mostly removed from the object frame. Finally, 1-dimensional spectral orders (pixel vs. flux) were extracted from the 2-dimensional frames.

We retrieved 47 orders of 4096 pixels each. No order merging was applied. The observation of the UVES Thorium-Argon (Th-Ar) lamp enabled us to assign each pixel the appropriate value of the wavelength. For each night, we used the Th-Ar spectrum observed before/after the science exposures and established an 8th order polynomial dispersion solution. All these data reduction steps were performed with the MIDAS software package.

5. Data analysis

After the data reduction, we identified cosmic-ray hits by way of the following procedure: for each spectrum, we compared the flux in every pixel with the median flux of the same pixel in the three predecessor and the three successor spectra, which had been scaled to the same flux as the spectrum under consideration. We flagged those pixels where the difference exceeded 6σ as cosmic-ray hits. These pixels were then excluded from further analysis. We furthermore discarded the most weakly exposed regions of each echelle order (the first 400 pixels as well as the last 240 pixels) since the flux level of the continuum was subjected to strong variations. In addition, the spectral order around the wavelength of $\lambda = 630 \text{ nm}$ was excluded from further analysis, since data were affected by the strong telluric OI features. In order to speed up the data analysis, we co-added spectra into sufficiently narrow phase bins in such a way that phase smearing of the stellar absorption lines originating from stellar RV variation, sub-pixel shifts and the effect of barycentric motion of the Earth remained negligible. The main criterion for the size of the phase bins was that the unseen planetary lines did not suffer from smearing in excess of 2 km s^{-1} . With that step, we were able to reduce the number of spectra from 406 to 58.

5.1. Data synthesis method

We model the starlight reflected from the planet as a copy of the stellar spectrum, strongly scaled down in brightness and Doppler-shifted according to the orbital motion of the planet. The target spectra have an average S/N of 300 to 600 per spectral bin. With expected planet-to-star flux ratios of the order of

Table 2. Journal of observations. The UTC times and the orbital phases of the planet are shown. Ephemerides used are: BJD 2451653.968 + 3.31245 \times E (Leigh et al. 2003a quoting Marcy priv. comm.).

Night	UTC start	BJD start	ϕ	UTC end	BJD end	ϕ	N_{spectra}
1	2007/06/16 23:24	2454268.4773	0.30	2007/06/17 04:12	2454268.6784	0.36	100
2	2007/06/17 22:45	2454269.4498	0.59	2007/06/18 04:26	2454269.6873	0.66	306

a few times 10^{-5} , it is clear that the reflected spectrum from the planet is deeply buried in the noise of the stellar spectrum. The weak planetary signal is boosted by the large number of spectra, and more importantly, by the combination of the approximately 1500 absorption lines, achieved using the data-synthesis method (cf. Charbonneau et al. 1999) described below in a nutshell (for a detailed description see Rodler et al. 2008).

In the first step, a high S/N, virtually planet-free superspectrum is computed by co-adding the observed spectra after correcting their wavelength values for the barycentric motion of the Earth and for the stellar orbital motion. Then, we construct a model to describe each of the original, unmodified object spectra: the dominant stellar signal is represented by the superspectrum, shifted to the position of the observed spectrum. Imperfections in flux and wavelength are corrected by using the approach described in Rodler et al. (2008). Furthermore, the contribution to the spectrum of the planetary signal is created as follows: we adopt the spectrum of the slowly rotating F6 IV star HD 136351 to mimic the expected sharp reflected lines of the planet (Section 3.2). For each observed object spectrum, we need to co-align that spectrum of HD 136351 with the stellar model spectrum (shifted superspectrum). The co-aligned spectrum of HD 136351 is then scaled down by the factor $\epsilon(\lambda) \mu(\phi, i)$ and shifted by velocity $V_p(K_p, \phi)$ with respect to the stellar spectrum. Hence, the two free parameters of the planetary model are the planet-to-star flux ratio for the fully-illuminated planet $\epsilon(\lambda)$, and the orbital inclination i , which corresponds to an RV semi-amplitude of the planet $K_p = K_{p,\text{max}} \sin i = 155.6 \sin i \text{ km s}^{-1}$. Concerning the albedo function $p(\lambda)$, we adopt (i) a grey albedo assumption (i.e. $p(\lambda) = \text{constant}$ for all wavelengths λ) and (ii) the irradiated atmospheric Class IV model by Sudarsky et al. (2000), which predicts higher reflectivity at shorter wavelengths (Fig. 2).

The search range for the RV semi-amplitude comprises $K_p = 40$ to 180 km s^{-1} (corresponding to orbital inclinations $i = 15^\circ$ to 90° , plus twice the error of $K_{p,\text{max}}$ (i.e. 18.3 km s^{-1} with a step width of 3 km s^{-1}). This is a good compromise between computing time and sampling the expected average reflected absorption line profile with the FWHM of $\approx 12 \text{ km s}^{-1}$. Since the tidal lock hypothesis and a spin-orbit alignment is very likely, low-inclination orbits can be furthermore excluded: the observed $v \sin i = 15 \text{ km s}^{-1}$ would imply an improbable true rotational velocity above 50 km s^{-1} for an F7 IV-V star at very low orbital inclinations (c.f. rotational velocities of late F-type stars; Glebocki & Stawikowski 2000). Using simulations, we found that for small inclinations of the planetary orbit, where the planets appear only slightly illuminated, and the method would fail to detect Jupiter-size objects even with very high albedos.

For the second parameter $\epsilon(\lambda_0)$, we search for the planetary signal in the range 10^{-4} to 10^{-5} with a step size of 5×10^{-6} .

5.2. Determination of the confidence level

Once the best model $M[K_p, \epsilon(\lambda)]$ has been evaluated, we determine the confidence level of the χ^2 minimum. We do not infer

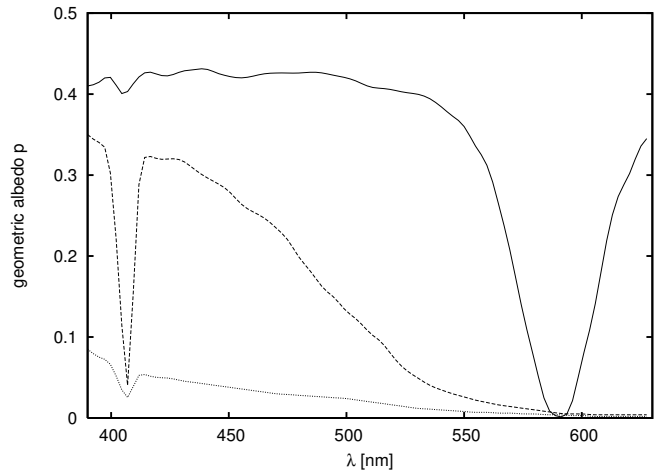


Fig. 2. Different albedo spectra of atmospheric models (taken from Sudarsky et al. 2000) are shown. The irradiated (dots) and isolated (dashed) Class IV models describe atmospheres of planets with temperatures $T_{\text{eff}} \approx 1300 \text{ K}$. Contrary to the isolated model, the irradiated model assumes that no reflective clouds exist in the upper layer of the planetary atmosphere, which results in a very low albedo. The solid line depicts a Class V roaster, describing the atmosphere of a planet with $T_{\text{eff}} \geq 1500 \text{ K}$, having a high reflective silicate cloud deck in the upper layers of the atmosphere. This atmospheric model was already ruled out for τ Boo b by Leigh et al. (2003a).

the confidence from the probability of the minimum χ^2 value, because due to unknown systematic errors coming from the telescope and instrument the true errors are largely underestimated when considering only photon statistics and detector read-out noise. Therefore no reasonable probability estimate is possible from the χ^2 value alone. For this reason, we apply the bootstrap randomization method (e.g. Kürster et al. 1997). Retaining the orbital phases, we randomly redistribute the observed spectra amongst the phases, thereby creating a large number ($N = 3000$) of different data sets. Any signal present in the original data is now scrambled in these artificial data sets. For all these randomised data sets, we again evaluate the model for the two free parameters, and locate the best fit with its specific χ^2 minimum. We set m to be the number of best-fit models to the N randomised data sets that have a minimum χ^2 less or equal than the minimum χ^2 found for the original data set. The confidence level can then be estimated by $1 - m/N$.

6. Results

6.1. Grey albedo model

Our data analysis adopting a grey albedo model resulted in a χ^2 -minimum at a planet-to-star flux ratio $\epsilon = 3.3 \times 10^{-5}$ and an RV semi-amplitude $K_p = 103 \text{ km s}^{-1}$ corresponding to an orbital inclination of $i = 41^\circ$. Figure 3 (upper panel) shows the χ^2 contour map in the ϵ vs. K_p plane. However, using bootstrap

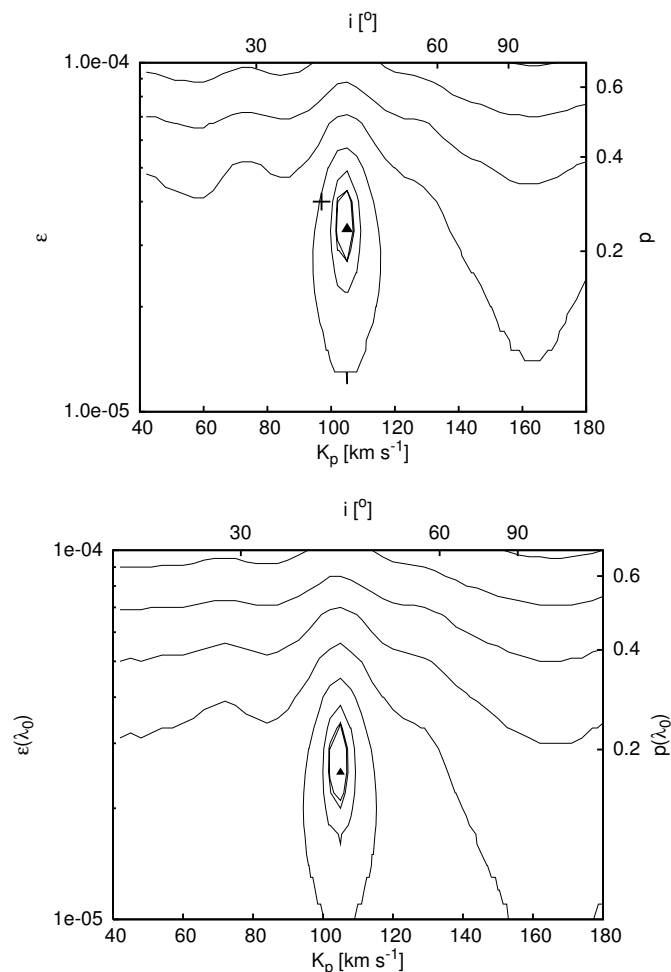


Fig. 3. Contour maps of χ^2 for the model parameters of the planet of K_p (RV semi-amplitude of the planet) and $\epsilon(\lambda_0)$ (planet-to-star flux ratio); this plot shows the result of the analysis of the τ Boo b data for two different atmospheric models. The contour levels follow the sequence $C_k = \chi^2_{\min} + 10^{-6}(\chi^2 - \chi^2_{\min})^3$ for $k > 0$, where χ^2_{\min} is the minimum χ^2 .

Upper panel: grey albedo model (model #1). Lower panel: irradiated Class IV albedo function (model #2). For both cases, a Venus-like phase function was adopted. The minimum χ^2 was found at $K_p = 103 \text{ km s}^{-1}$ and $\epsilon = 3.3 \times 10^{-5}$, and $K_p = 103 \text{ km s}^{-1}$ and $\epsilon(\lambda_0) = 2.5 \times 10^{-5}$, respectively, for model #1 and model #2. A bootstrap analysis with 3000 trials revealed that these features are uncertain with a false alarm probability of 3.6% and 7.3%, respectively, for model #1 and model #2. For comparison, we show the candidate feature found by Leigh et al. (2003a) at $K_p = 97 \text{ km s}^{-1}$ and $\epsilon = 4 \times 10^{-5}$, assuming the grey albedo case (upper panel, cross). This candidate feature has a FAP of 1.4%. Note that the corresponding geometric albedo p is shown under the assumption that $R_p = 1.2 R_{\text{Jup}}$ (the right-hand y-axis).

randomisation with 3000 trial data sets we find this χ^2 -minimum to be uncertain with a false alarm probability (FAP) of 3.6%, and consequently do not consider it as a detection of reflected light from the planet.

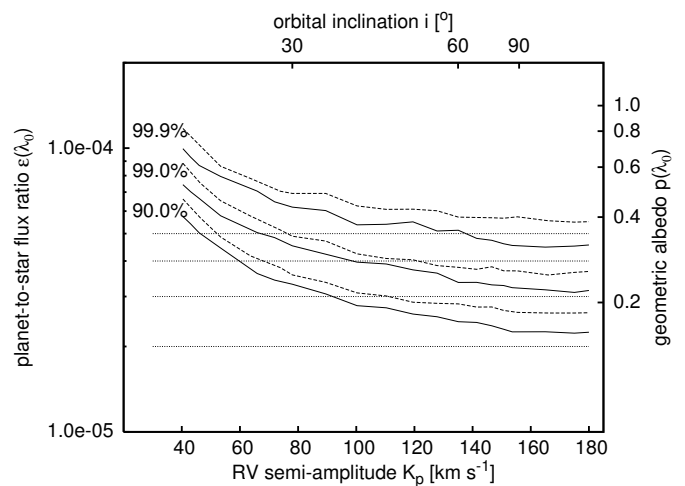


Fig. 4. Contour map showing confidence levels for the upper limits to the planet-to-star flux ratio $\epsilon(\lambda_0)$ as a function of the RV semi-amplitude K_p of the planet (lower x-axis), or orbital inclination i (upper x-axis). From top to bottom, these levels are: 99.9, 99.0 and 90.0 % confidence. For the planetary model we assumed a Venus-like phase function as well as a irradiated Class IV albedo function (dashed lines) and a grey albedo (solid lines). The corresponding geometric albedo p is shown under the assumption that $R_p = 1.2 R_{\text{Jup}}$ (the right-hand y-axis).

6.2. Irradiated Class IV model function

The analysis with the irradiated Class IV albedo model did not yield any evidence for reflected light either. We find the formal χ^2 -minimum at a planet-to-star flux ratio $\epsilon(\lambda_0) = 2.5 \times 10^{-5}$ and an RV semi-amplitude of $K_p = 103 \text{ km s}^{-1}$, which again corresponds to an orbital inclination $i = 41^\circ$. Figure 3 (lower panel) shows the χ^2 contour map in the ϵ vs. K_p plane. From bootstrap randomisation with 3000 trials we found this feature to be uncertain with a FAP of 7.3%.

6.3. Upper limits

Given the non-detection of the planetary signal, we determined upper limits of the planet-to-star flux ratio $\epsilon(\lambda_0)$ for different confidence levels as a function of the RV semi-amplitude K_p . Figure 4 shows that the upper limits to the planet-to-star flux ratio decrease with increasing orbital inclination, which is a direct consequence of the illumination geometry. As can be seen from Figure 4 (solid lines), we have the highest sensitivity for detection of the planetary signal at high orbital inclinations. For the most probable orbital inclination of 46° , the 99.9 % confidence upper limit to the planet-to-star flux ratio for the grey albedo model is $\epsilon = 5.7 \times 10^{-5}$, while it is $\epsilon = 6.5 \times 10^{-5}$ for the irradiated Class IV albedo function. For an orbital inclination of $i = 60^\circ$, the 99.9 % confidence upper limit to the planet-to-star flux ratio for the grey albedo model is already $\epsilon = 5.1 \times 10^{-5}$, while it is $\epsilon = 5.7 \times 10^{-5}$ when adopting the irradiated Class IV albedo function. Similar to our results for the hot Jupiter HD 75289Ab (Rodler et al. 2008), Figure 4 shows that the upper limits established by adopting the grey albedo model are deeper than the ones found with the irradiated Class IV model.

Assuming a planetary radius $R_p = 1.2 R_{\text{Jup}}$ and an orbital inclination $i \approx 46^\circ$ (cf. Section 3), we find the upper limit to the geometric albedo to be $p < 0.40$ for the grey albedo model and

$p < 0.44$ for the irradiated Class IV model at a wavelength of $\lambda_0 = 462$ nm, which corresponds to the centre of gravity of the irradiated Class IV albedo function in the observed wavelength range. For comparison, at this wavelength Jupiter's geometric albedo is $p = 0.44$ (Karkoschka 1994).

7. Discussion and conclusions

We have observed the hot Jupiter orbiting τ Boo for two half nights with UVES, mounted at the VLT/UT2, in an attempt to measure starlight reflected from the planetary companion.

- The data analysis using the data synthesis method did not reveal a detection of the reflected light from the planet. The signal-to-noise ratio of the combined data was not sufficient to significantly detect the planetary signal; instead we placed upper limits to the planet-to-star flux ratio for different possible orbital inclinations and confidence levels. Under the assumption of a planetary radius of $R_p = 1.2 R_{\text{Jup}}$, we rule out atmospheric models with geometrical albedos $p > 0.40$ for τ Boo b. We confirm the finding by Leigh et al. (2003a) that the upper limit to the geometric albedo of the planet (e.g. $p < 0.39$ for orbital inclinations $i \geq 36^\circ$ and grey albedo) implies that this planet has a lower reflectivity than the atmospheres of Jupiter ($p = 0.44$) and Saturn ($p = 0.62$).
- For both albedo models, we find a formal χ^2 -minimum at $K_p = 103 \text{ km s}^{-1}$. For the analysis adopting the irradiated Class IV albedo model, we determine the FAP of the candidate feature to be 7.3%. In comparison, Leigh et al. (2003a) finds a candidate feature of marginal significance (FAP=0.9%) with $K_p = 90 \text{ km s}^{-1}$. For the analysis adopting the grey albedo model, we find that this candidate feature has a low FAP of 3.6% with a planet-to-star flux ratio of $\epsilon = 3.3 \times 10^{-5}$. If genuine, this would correspond to an orbital inclination of $i = 41^\circ$ and a geometric albedo of $p = 0.23$ assuming $R_p = 1.2 R_{\text{Jup}}$. For the grey albedo model, Leigh et al. (2003a) reports about the detection of a non-significant candidate feature with a similar value of $K_p = 97 \text{ km s}^{-1}$, having a low FAP of 1.4%. These similar, but non-significant candidate features were found by using completely independent data sets and data analysis methods. Leigh et al. (2003a) analyzed high-resolution spectroscopic data, which had been obtained during 17 nights with the Utrecht Echelle Spectrograph (UES), mounted on the William Herschel-telescope in La Palma, Spain. Contrary to our analysis strategy, they used a deconvolution approach (Collier Cameron et al. 2002) for the extraction of the planetary signal. In this work, we analyzed UVES data, obtained during two half nights, by using the data synthesis method. These results are also consistent with an estimate of the orbital inclination of $i \approx 46^\circ$ (corresponding to a semi-amplitude of $K_p = 112 \text{ km s}^{-1}$) and assuming tidal locking. Leigh et al. (2003a) achieves a higher sensitivity by adopting the irradiated Class IV model atmosphere, whereas our highest sensitivity is attained with the grey albedo assumption. One explanation for this might be that Leigh et al. (2003a) were using data with a slightly better wavelength coverage at blue wavelengths (407–647 nm), while our data set covered the wavelength range from 425 to 632 nm. However, it seems to be more likely that this discrepancy between the best-fit atmospheric models is just coincidence, since both campaigns resulted only in non-significant candidate features.

Acknowledgements. We are very grateful to Tsevi Mazeh for valuable discussions.

References

- Alonso R., Alapini A., Aigrain S., et al., 2009a, *A&A*, 506, 353
 Alonso R., Guillot T., Mazeh T., et al., 2009b, *A&A*, 501, 23
 Bakos G., Noyes R., Kovács G., Latham D., et al. 2007, *ApJ Letters*, 656, 552
 Baliunas S., Henry G. W., Donahue R. A., Fekel F. C., & Soon W. H. 1997, *ApJ*, 474, L119
 Butler R. P., Marcy G. W., Williams E., et al. 1997, *ApJ*, 474, L115
 Butler R. P., Wright J. T., Marcy G. W., Fischer D. A., Vogt S. S., Tinney, C. G., 2006, *ApJ*, 646, 505
 Charbonneau D., Noyes R.W., Korzennik S.G., Nisenson P., Jha S., Vogt S.S., & Kibrik R.I., 1999, *ApJ*, 522, L145
 Cameron A. C., Horne K., Penny A., James D. 1999, *Nature*, 378, 355
 Christiansen J. L., Ballard S., Charbonneau D., et al., 2010, *ApJ*, 710, 97
 Collier Cameron A., Horne K., Penny A., Leigh C. 2002, *MNRAS*, 330, 187
 Cowan N. B. & Agol E., 2010, arXiv:1001.0012
 Dekker H., D'Odorico S., Kaufer A., et al., 2000, *SPIE*, 4008, 534.
 Eggenberger A., Udry S., & Mayor M. 2003, *ASP Conf. Ser.*, 294, 43
 Fabricky & Winn 2009, arXiv: 0902.0737
 Glebocki R. & Stawikowski A., 2000, *AcA*, 50, 509
 Gonzalez G. 1998, *A&A*, 334, 221
 Gratton R. G., Focardi P., Bandiera R., 1989, *MNRAS*, 237, 1085
 Gray, 1992, "The observation and analysis of stellar photospheres", *Camb. Astrophys. Ser.*, Vol. 20 *Astrophysics*
 Henry G. W., Baliunas S. L., Donahue R. A., et al., 2000, *ApJ*, 531, 415
 Hilton, J.L., 1992, *Explanatory Supplement to the Astronomical Almanac*, University Science Books, Mill Valley CA, p. 383
 Hoffleit D. & Jaschek C., 1991, *The Bright star catalogue*, Yale University Observatory, New Haven, Connecticut
 Karkoschka E., 1994, *Icarus*, 111, 174
 Knutson H., Charbonneau D., Allen L. E., et al. 2007, *Nature*, 447, 183
 Kürster M., Schmitt J.H.M.M., Cutispoto G., Dennerl K., 1997, *A&A*, 320, 831
 Latham D. W., Stefanik R. P., Mazeh T. Mayor M. & Burki G. 1989, *Nature*, 339, 38
 Leigh C., Collier Cameron A., Horne K., Penny A., James D., 2003a, *MNRAS*, 344, 1271
 Leigh C., Collier Cameron A., Udry S., Donati J.-F., Horne K., James D., Penny A. 2003b, *MNRAS*, 346, 16
 McLaughlin D. B. 1924, *ApJ*, 60, 22
 Narita N., Sato Bunéi H. T., Tamura M., 2009, *PASJ*, 61, L35
 Patience J., White R. J., Ghez A. M., et al. 2002, *ApJ*, 581, 654
 Pont F., Hébrard G., Irwin J. M., Bouchy F., 2009, *A&A*, 502, 695
 Reiners A. & Schmidt J. H. M. M. 2003, *A&A*, 412, 813
 Rodler F., Kürster M., Henning T. 2008, *A&A*, 485, 859
 Rogers J. C., Apai D., López-Morales M., et al., 2009, *ApJ*, 707, 1707
 Rossiter R. A. 1924, *ApJ*, 60, 15
 Rowe J. F., Matthews J. M., Seager S., et al., 2008, *ApJ*, 689, 1345
 Seager S. & Sasselov D. D., 1998, *ApJ*, 502, 157
 Shkolnik E., Walker G. A. H., Bohlender D. A., Gu P.-G., Krster M., 2005, *ApJ*, 622, 1075
 Snellen I. A. G., de Mooij E. J. W., Albrecht, S., 2009, *Nature*, 459, 543
 Sing D. K. & López-Morales M., 2009, *A&A*, 493, 31
 Sudarsky D., Burrows, A., Pinto P., 2000, *ApJ*, 538, 885
 Sudarsky D., Burrows A., Hubeny I., 2003, *ApJ*, 588, 1121
 Valenti J. A., Fischer D. A., 2005, *ApJ Supl.*, 159, 141